Iridium-based Metallo-organic Triangles as Efficient Singlet Oxygen Photosensitizers for Rhodamine B Photodegradation

Xiaojie Huang,[a‡] Yuxin Li,[a‡] Min Wang,[c] Ning Wang,[a] Jun Wang,[a] Pingshan Wang,*[a,b] Mingzhao Chen,*[a] Zhilong Jiang*[a]

Table of Contents

1. General Procedures

All starting materials were purchased from Aldrich, Alfa Aesar and used without further purification. Column chromatography was conducted by using basic A**L2**O_3 (sinopharm chemical reagents co., Ltd, 200-300 mesh) or SiO_2 (Qingdao Haiyang Chemical co., Ltd, 200-300 mesh). The ^1H NMR and ^{13}C NMR spectra were recorded on a Bruker Avance 400-MHz and 500-MHz NMR spectrometer in $CDCl_3$, and CD_3CN with TMS as the inner standard.

ESI. ESI mass spectrometry and traveling wave ion mobility (TWIM) experiments were conducted on a Waters Synapt HDMS G2i instrument with a LockSpray ESI source, using the following parameters: ESI capillary voltage, 1.3-3.0 kV; sample cone voltage, 20-25 V; extraction cone voltage, 1.1-3 V; desolvation gas flow, 800 L/h (N_2); trap collision energy (CE), 4 V; transfer CE, 0 V; trap gas flow, 2.0 mL/min (Ar); source temperature, 30 °C; and desolvation temperature, 30 °C. All samples were dissolved in CH_3CN or CH_3CN/CH_3NO_2 (1:1, v/v) and then infused into the -100, KD Scientific). Data were collected and analyzed by using MassLynx 4.1 and DriftScope 2.4 (Waters).

2. Synthesis of ligands and complexes

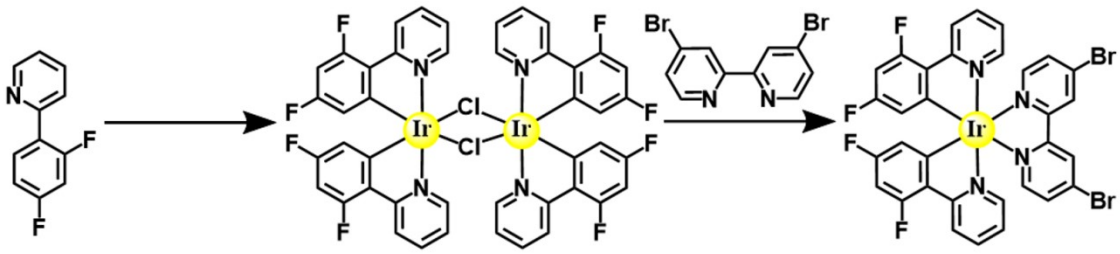

1 **2**

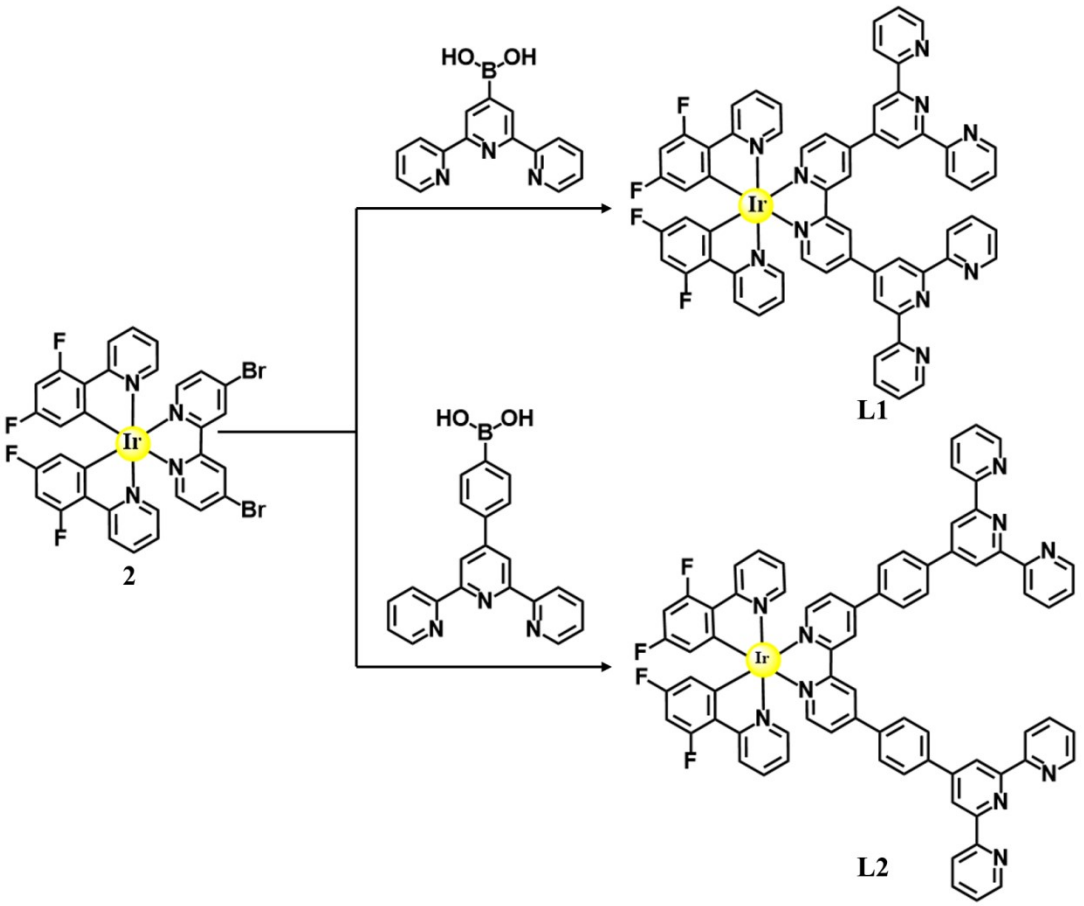

Scheme S1: The synthetic route of ligands **L1** and **L2**.

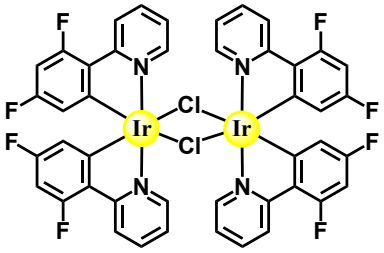

Compound **1**[1]: 2-(2,4-Difluorophenyl)pyridine (250 mg, 0.71 mmol) and $IrCl_3 \cdot xH_2O$ (340 mg, 1.78 mmol) were added to a 500 mL flask, then 2-Ethoxyethanol (120 mL) and H_2O (40 mL) was added, heating the system to reflux at 110 °C under nitrogen for 24 h. After cooled to ambient temperature, the precipitates were filtered and washed with MeOH to afford compound 340 mg, 62.9 %. ^{1}H NMR (400 MHz, DMSO-d_6) δ 9.79 (d, J = 5.0 Hz, 2H), 9.56 (d, J = 4.9 Hz, 2H), 8.30 (s, 2H), 8.25 (s, 2H), 8.21 (s, 2H), 8.13 (s, 2H), 7.67 (s, 2H), 7.58 (s, 2H), 6.90 -6.76 (m, 4H), 5.73 (d, J = 8.5 Hz, 2H), 5.07 (d, J = 8.7 Hz, 2H).

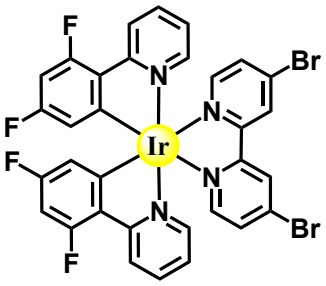

Compound **2**[1]**:** Added compound **1** (300 mg, 0.25 mmol) and 4,4'-Dibromo-2,2'-bipyridyl (180 mg, 0.55mmol), MeOH (100 mL) and CH_2Cl_2 (100 mL) to a 250 mL flask, heated to reflux at 50 °C for 12 h. After cooled to ambient temperature, purified by column chromatograph with neutral Al_2O_3 (200-300 mesh) with DCM and MeOH as eluent, a yellow powder was generated: 296 mg, 66.78 %. ^{1}H NMR (400 MHz, CD_3CN) δ 10.33 (d, J = 1.8 Hz, 2H, H^m), 9.70 (ddt, J = 8.5, 2.3, 1.1 Hz, 2H, H^j), 9.31 (td, J = 8.0, 1.6 Hz, 2H, H^f), 9.20 – 9.14 (m, 4H, H^k, H^e), 9.08 – 9.02 (m, 2H, H^l), 8.50 (ddd, J = 7.4, 5.8, 1.4 Hz, 2H, H^i), 8.07 (ddd, J = 12.7, 9.3, 2.4 Hz, 2H, H^c), 7.04 (dd, J = 8.5, 2.4 Hz, 2H, H^a). ESI-MS (1031.51 calcd. For $C_{32}H_{18}Br_2F_{10}IrN_4P$ with PF_6^-): m/z 886.9506 $[M–PF_6^-]^+$ (calcd m/z: 886.9518).

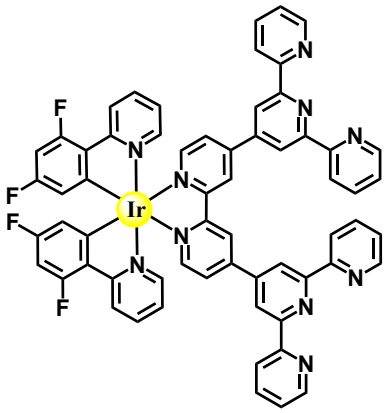

Ligand **L1:** To a flask containing a mixture of compound **2** (70 mg, 0.059 mmol), 2,6-di(pyridin-2-yl)pyridin-4-yl-4-boronic acid (87 mg, 0.32 mmol) and K_2CO_3 (48 mg, 0.35 mmol), CH_3CN (100 mL), CH_3OH (10 mL) and H_2O (10 mL) were added. The system was degassed for 10 min, and $Pd(PPh_3)_4$ (14 mg, 0.012 mmol) as the catalyst was added. The mixture was stirred at 85 °C under nitrogen for 72 h. After cooling to ambient temperature, the solvent was evaporated *in vacuo* and the residue was purified by column chromatography (Al_2O_3), eluting with a mixture of MeOH and CH_2Cl_2. The

complex was obtained, as a yellow precipitate: 215 mg, 78.5 %. ^{1}H NMR (400 MHz, CD_3CN) δ 9.23 (d, J = 1.9 Hz, 2H, H^{m}), 8.91 (s, 4H, tpy-$H^{3',5'}$), 8.76 – 8.70 (m, 8H, tpy-$H^{3,3''}$, tpy-$H^{6,6''}$), 8.40 (d, J = 8.4 Hz, 2H, H^{j}), 8.21 (d, J = 5.8 Hz, 2H, H^{k}), 8.05 – 7.94 (m, 8H, H^{e}, H^{f}, tpy-$H^{4,4''}$), 7.81 (dd, J = 5.6, 1.5 Hz, 2H, H^{l}), 7.48 (ddd, J = 7.5, 3.7, 1.0 Hz, 4H, tpy-$H^{5,5''}$), 7.18 (ddd, J = 7.4, 5.8, 1.4 Hz, 2H, H^{i}), 6.78 (ddd, J = 12.2, 9.5, 2.4 Hz, 2H, H^{c}), 5.84 (dd, J = 8.6, 2.4 Hz, 2H, H^{a}). ^{19}F NMR (471 MHz, CD_3CN) δ -107.94 (d, 2F, ortho), -109.90 (d, 2F, para). ESI-MS (1336.23 calcd. For $C_{62}H_{38}F_{10}IrN_{10}P$ with PF_6^-): m/z 1191.2900 $[M–PF_6^-]^+$ (calcd m/z: 1191.2908).

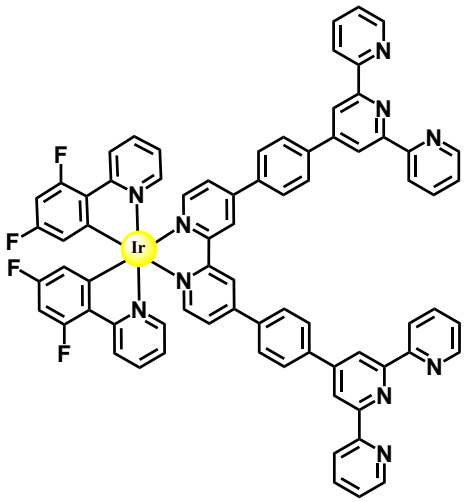

Ligand **L2:**Compound **2** (70 mg, 0.059 mmol) and 4′-(4-boronatophenyl)[2,2′:6′,2″]terpyridine (87 mg, 0.25 mmol) were added to a 250 mL flask, then CH_3CN: H_2O: CH_3OH (120 mL, V:V:V, 10:1:1) and K_2CO_3 (48 mg, 0.35 mmol) were added, The system was degassed for 10 min, and $Pd(PPh_3)_4$ (14 mg, 0.012 mmol) as the catalyst was added. The mixture was stirred at 85 °C under nitrogen for 72 h, after cooled to ambient temperature, purified by column chromatograph with neutral Al_2O_3(200-300 mesh) with DCM and MeOH as eluent, a yellow powder was generated: 215 mg, 78.5 %. ^{1}H NMR (400 MHz, CD_3CN) δ 8.93 (d, J = 1.9 Hz, 2H, H^{m}), 8.74 (s, 4H, tpy-$H^{3',5'}$), 8.68 – 8.59 (m, 8H, tpy-$H^{3,3''}$, tpy-$H^{6,6''}$), 8.30 (d, J = 8.5 Hz, 2H, H^{j}), 8.05 (s, 8H, H^{g}, H^{h}), 8.00 (d, J = 5.8 Hz, 2H, H^{k}), 7.94 – 7.83 (m, 6H, H^{f}, tpy-$H^{4,4''}$), 7.78 (dd, J = 5.9, 1.9 Hz, 2H, H^{e}), 7.72 (d, J = 5.9 Hz, 2H, H^{l}), 7.37 (ddd, J = 7.5, 4.7, 1.2 Hz, 4H, tpy-$H^{5,5''}$), 7.12 – 7.04 (m, 2H, H^{i}), 6.67 (ddd, J = 12.2, 9.3, 2.5 Hz, 2H, H^{c}), 5.73 (dd, J = 8.5, 2.4 Hz, 2H, H^{a}). ^{19}F NMR (471 MHz, CD_3CN) δ -108.18 (d, 2F, ortho), -110.06 (d, 2F, para). ESI-MS (1488.43 calcd. For $C_{74}H_{46}F_{10}IrN_{10}P$ with

PF_6^-): m/z 1343.3596 $[M–PF_6^-]^+$ (calcd m/z: 1343.3527).

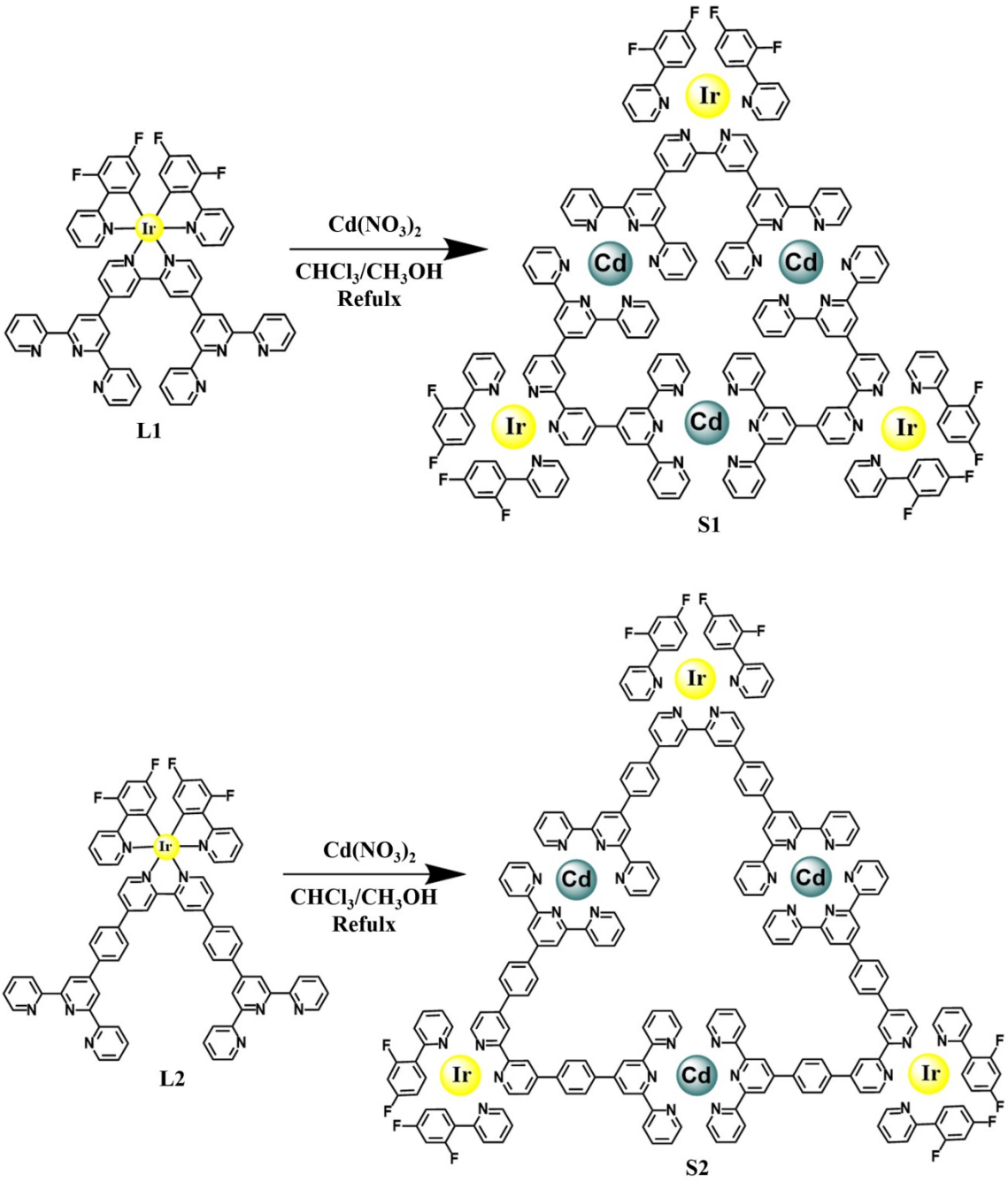

Scheme S2: The synthetic route of metallo-organic triangles **S1** and **S2**.

Triangle **S1**: Ligand **L1** (3.18 mg, 2.38 umol) and $Cd(NO_3)_2$•$4H_2O$ (0.74 mg, 2.39 μmol) were added into a 100 mL flask, then a solvent mixture of $CHCl_3/CH_3OH$ (20 mL, v/v, 1:1) was added. The mixture was refluxed for 12 h. After cooled to ambient temperature, excess NH_4PF_6 in CH_3OH was added to get a black precipitate, which was filtered and washed with CH_3OH to generate a light yellow solid: 3.81 mg, yield 92%. ^{1}H NMR (600 MHz, CD_3CN) δ 9.43 (s, 6H, H^m), 9.11 (s, 12H, tpy-$H^{3',5'}$), 8.80-8.79 (d,

J = 15 Hz, 12H, tpy-$H^{3,3''}$), 8.48-8.47 (d, *J* = 15 Hz, 6H, H^{j}), 8.43-8.42 (d, *J* = 15 Hz, 6H, H^{k}), 8.28-8.27 (d, *J* = 15 Hz, 6H, H^{l}), 8.23-8.20 (m, *J* = 24 Hz, 12H, tpy-$H^{4,4''}$), 8.14-8.13 (d, *J* = 15 Hz, 12H, tpy-$H^{6,6''}$), 8.06-8.03 (m, *J* = 21 Hz, 6H, H^{i}), 7.88-7.87 (m, *J* = 18 Hz, 6H, H^{e}), 7.49-7.47 (m, *J* = 21 Hz, 12H, tpy-$H^{5,5''}$), 7.24-7.22 (m, *J* = 21 Hz, 6H, H^{f}), 6.87-6.84 (m, *J* = 24 Hz, 6H, H^{c}), 5.92-5.90 (d, *J* = 15 Hz, 6H, H^{a}). ^{19}F NMR (471 MHz, CD_3CN) δ -107.73 (d, 6F, ortho), -109.74 (d, 6F, para). ESI-MS (5226.29 calcd. for $C_{186}H_{120}Cd_3F_{66}Ir_3N_{30}P_9$ with PF_6^-): m/z 1595.81 $[M–3PF_6^-]^{3+}$ (calcd m/z:1595.80) , 1160.60 $[M–4PF_6^-]^{4+}$ (calcd m/z: 1160.61) , 899.50 $[M–5PF_6^-]^{5+}$ (calcd m/z: 899.49) , 725.42 $[M–6PF_6^-]^{6+}$ (calcd m/z: 725.41).

Triangle **S2**: Ligand **L2** (3.54 mg, 2.38 umol) and $Cd(NO_3)_2•4H_2O$ (0.74 mg, 2.39 μmol) were added into a 100 mL flask, then a solvent mixture of $CHCl_3/CH_3OH$ (20 mL, v/v, 1:1) was added. The mixture was refluxed for 12 h. After cooled to ambient temperature, excess NH_4PF_6 in CH_3OH was added to get a black precipitate, which was filtered and washed with CH_3OH to generate a yellow solid: 3.07 mg, yield 91%. ^{1}H NMR (600 MHz, CD_3CN) δ 9.14 (s, 6H, H^{m}), 9.04 (s, 12H, tpy-$H^{3',5'}$), 8.83-8.81 (d, *J* = 18 Hz, 12H, tpy-$H^{3,3''}$), 8.46-8.41 (m, *J* = 36 Hz, 18H, H^{g}, H^{l}), 8.33-8.32 (d, *J* = 15 Hz, 12H, H^{h}), 8.26-8.24 (m, *J* = 18 Hz, 12H, tpy-$H^{4,4''}$), 8.21-8.20 (d, *J* = 12 Hz, 6H, H^{j}), 8.16-8.15 (d, *J* = 15 Hz, 12H, tpy-$H^{6,6''}$), 8.04-8.01 (d, *J* = 27 Hz, 12H, H^{k}, H^{i}), 7.86-7.85 (d, *J* = 12 Hz, 6H, H^{e}), 7.56-7.53 (m, *J* = 21 Hz, 12H, tpy-$H^{5,5''}$), 7.23-7.21 (m, *J* = 15 Hz, 6H, H^{f}), 6.84-6.80 (m, *J* = 24 Hz, 6H, H^{c}), 5.89-5.87 (d, *J* = 15 Hz, 6H, H^{a}). ^{19}F NMR (471 MHz, CD_3CN) δ -108.00 (d, 6F, ortho), -109.95 (d, 6F, para). ESI-MS (5678.36 calcd. for $C_{222}H_{144}Cd_3F_{66}Ir_3N_{30}P_9$ with PF_6^-): m/z 990.73 $[M–5PF_6^-]^{5+}$ (calcd m/z: 990.73) , 801.45 $[M–6PF_6^-]^{6+}$ (calcd m/z: 801.45) , 666.25 $[M–7PF_6^-]^{7+}$ (calcd m/z: 666.24) , 564.84 $[M–8PF_6^-]^{8+}$ (calcd m/z: 564.84).

3. ^{1}H NMR, ^{13}C NMR, 2D COSY and 2D NOESY spectra of ligands and complexes.

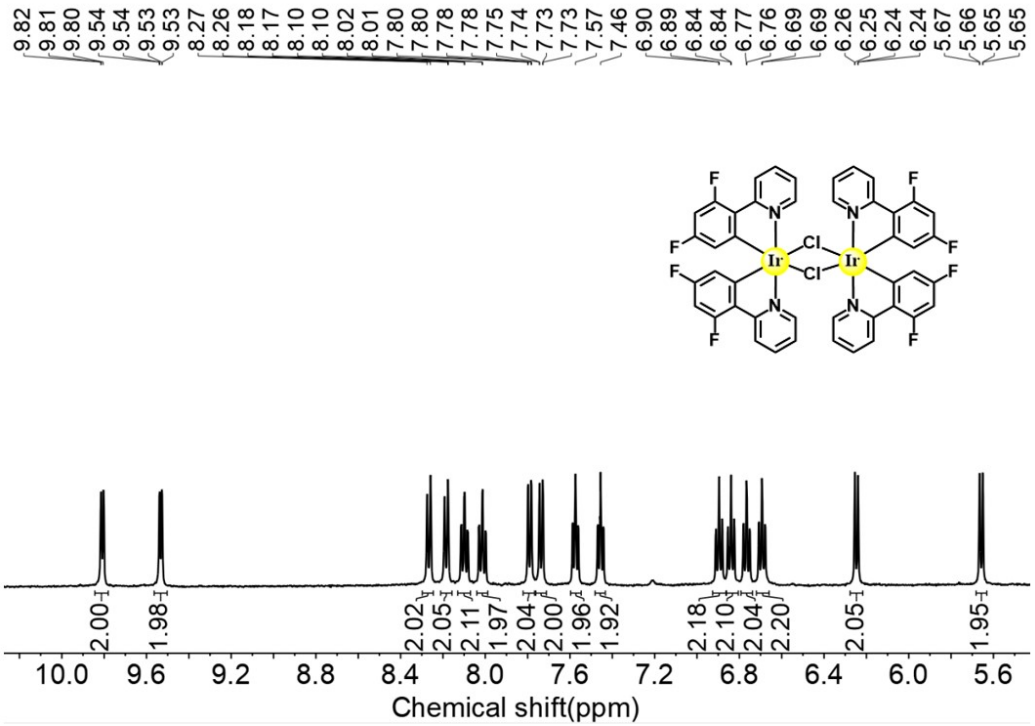

Figure **S1**: ^{1}H NMR spectrum (400 MHz) of compound **1** in DMSO-d_6.

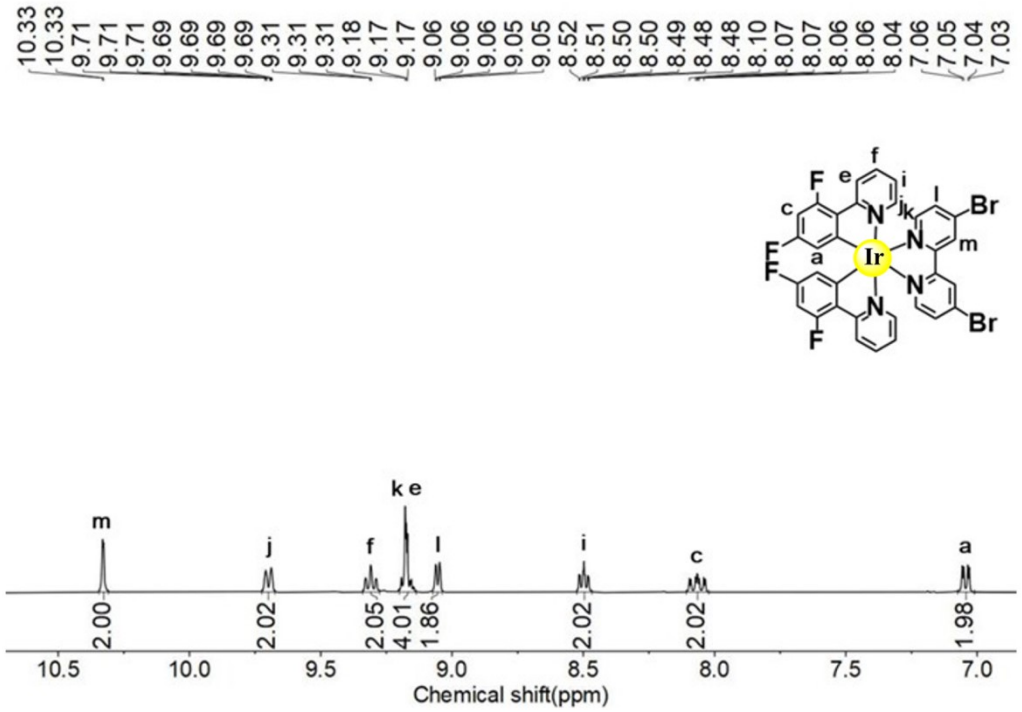

Figure **S2**: ^{1}H NMR spectrum (400 MHz) of compound **2** in CD_3CN.

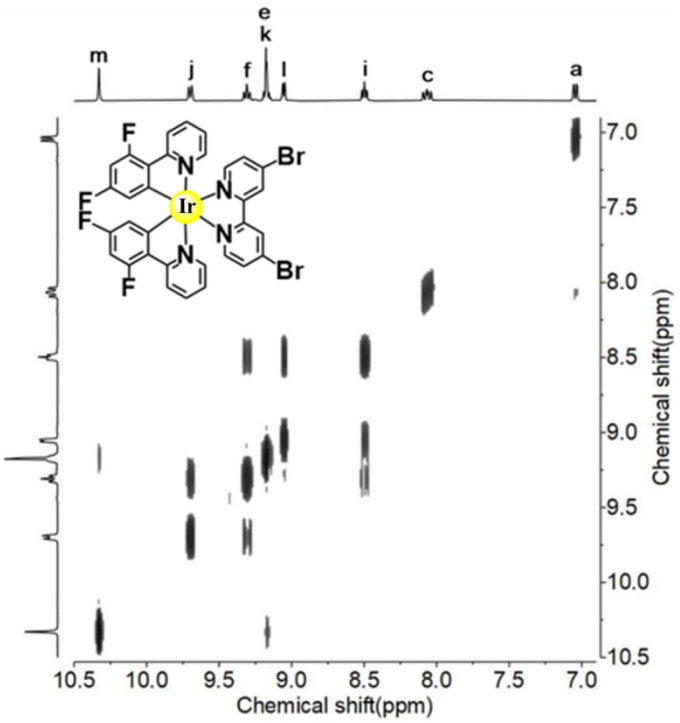

Figure **S3**: 2D COSY spectrum (400 MHz) of compound **2** in CD_3CN.

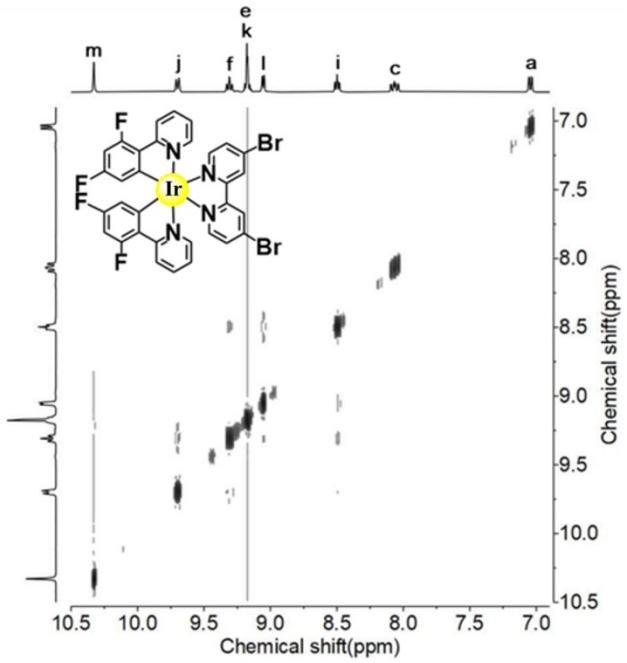

Figure **S4**: 2D NOESY spectrum (400 MHz) of compound **2** in CD_3CN.

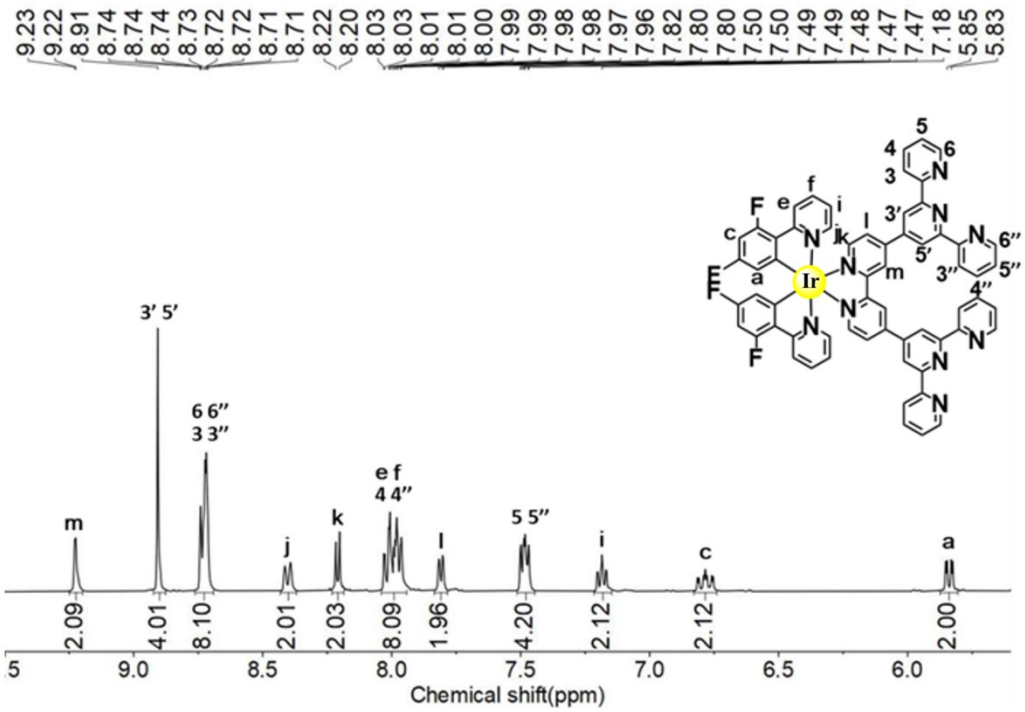

Figure **S5**: ^{1}H NMR spectrum (400 MHz) of ligand **L1** in CD_3CN.

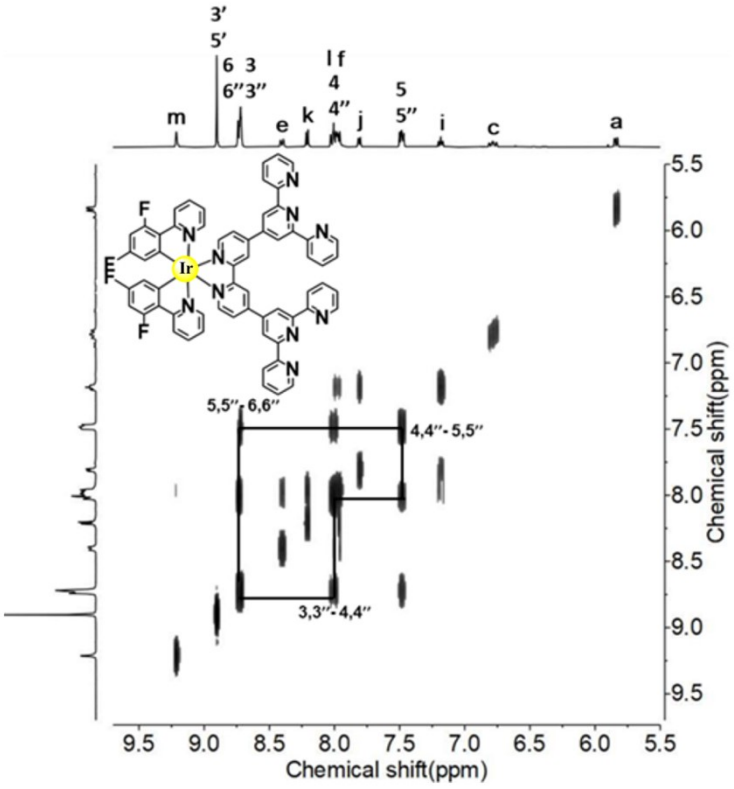

Figure **S6**: 2D COSY spectrum (400 MHz) of ligand **L1** in CD_3CN.

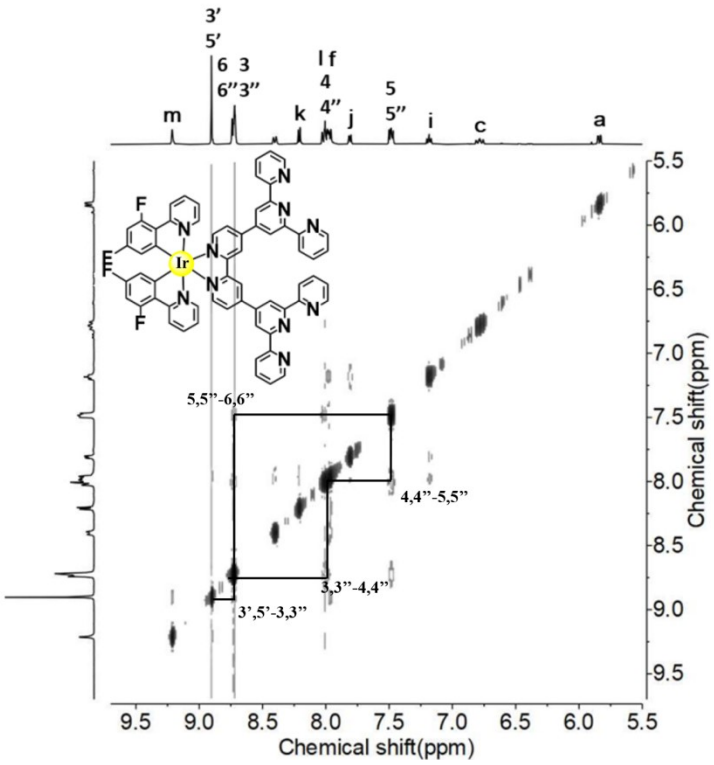

Figure **S7**: 2D NOESY spectrum (400 MHz) of ligand **L1** in CD_3CN.

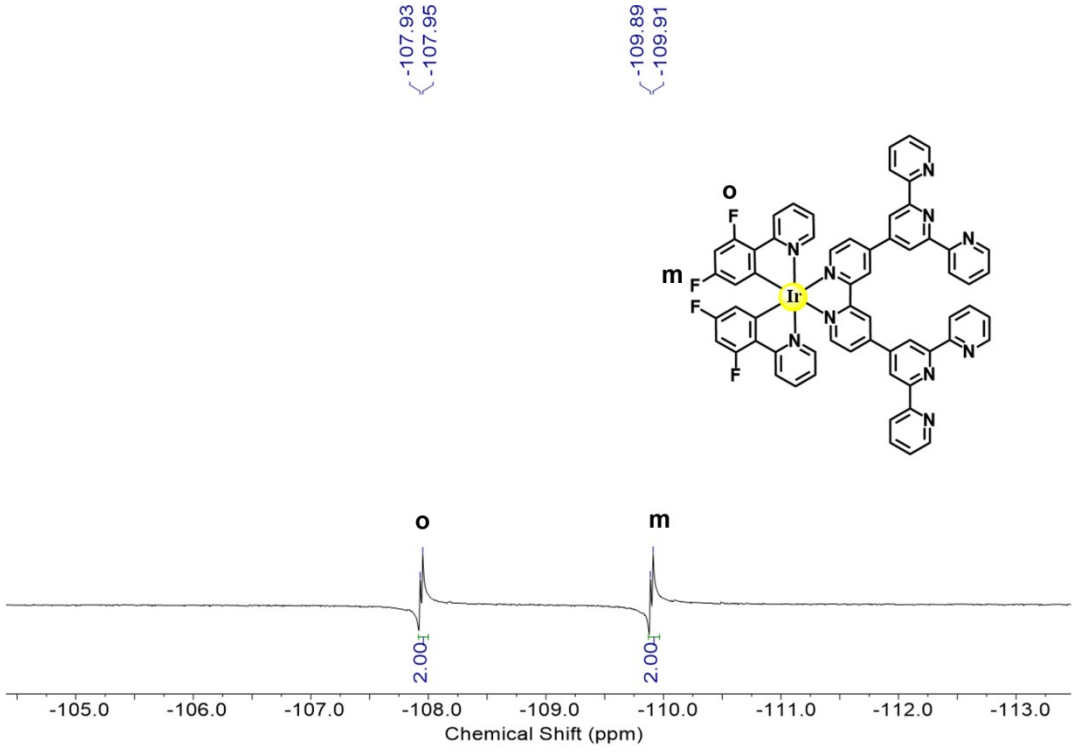

Figure **S8**: ^{19}F NMR spectrum (471 MHz) of ligand **L1** in CD_3CN.

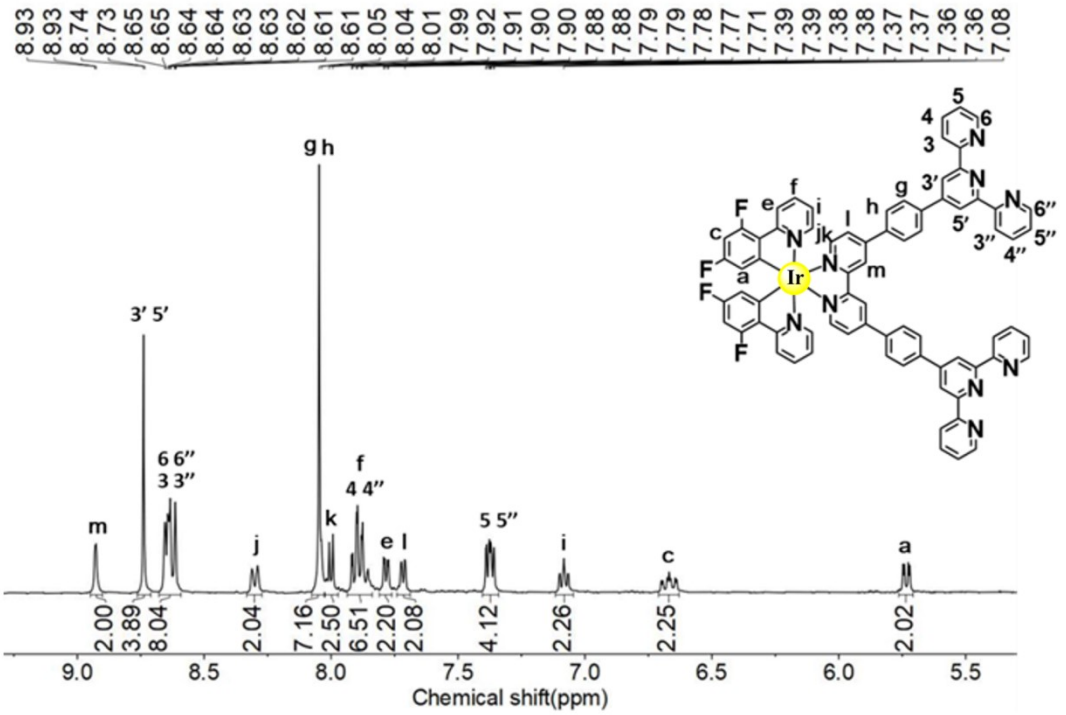

Figure **S9**: ^{1}H NMR spectrum (400 MHz) of ligand **L2** in CD_3CN.

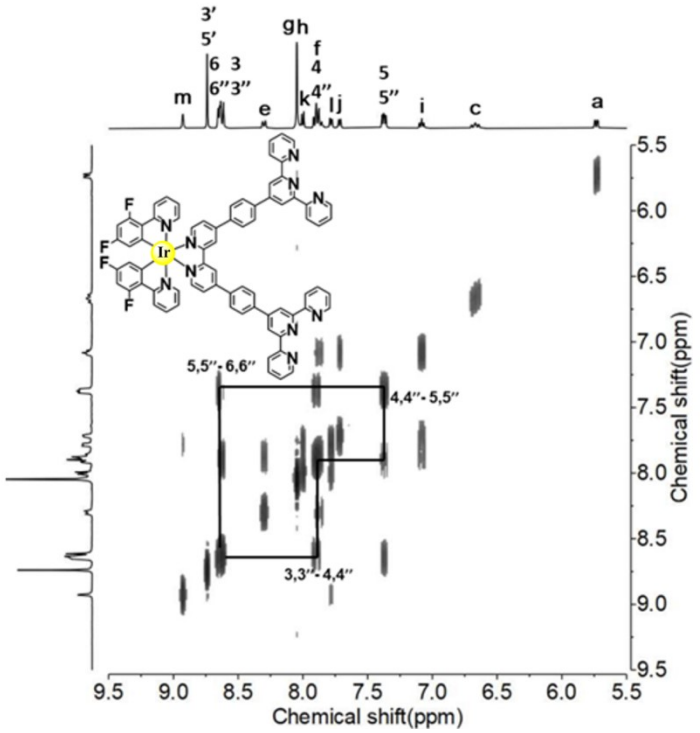

Figure **S10**: 2D COSY spectrum (400 MHz) of ligand **L2** in CD_3CN.

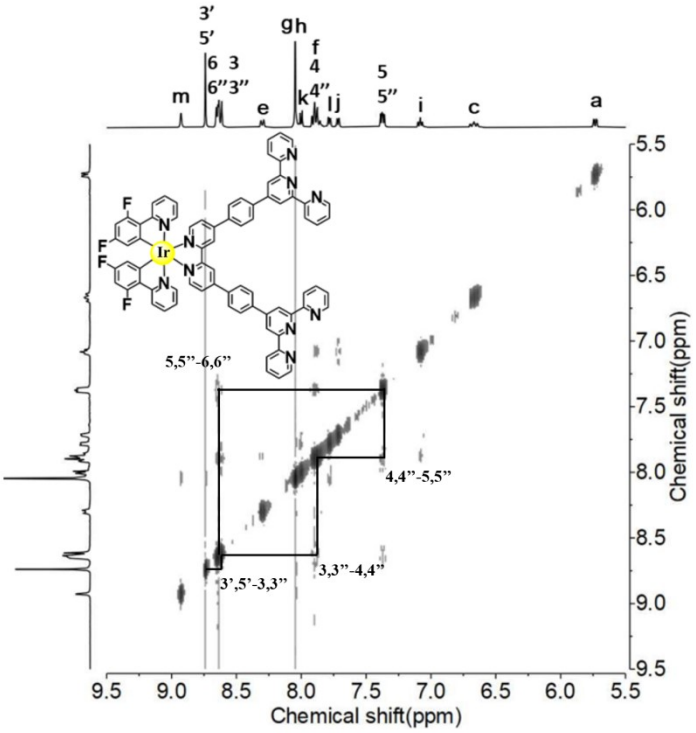

Figure **S11**: 2D NOESY spectrum (400 MHz) of ligand **L2** in CD_3CN.

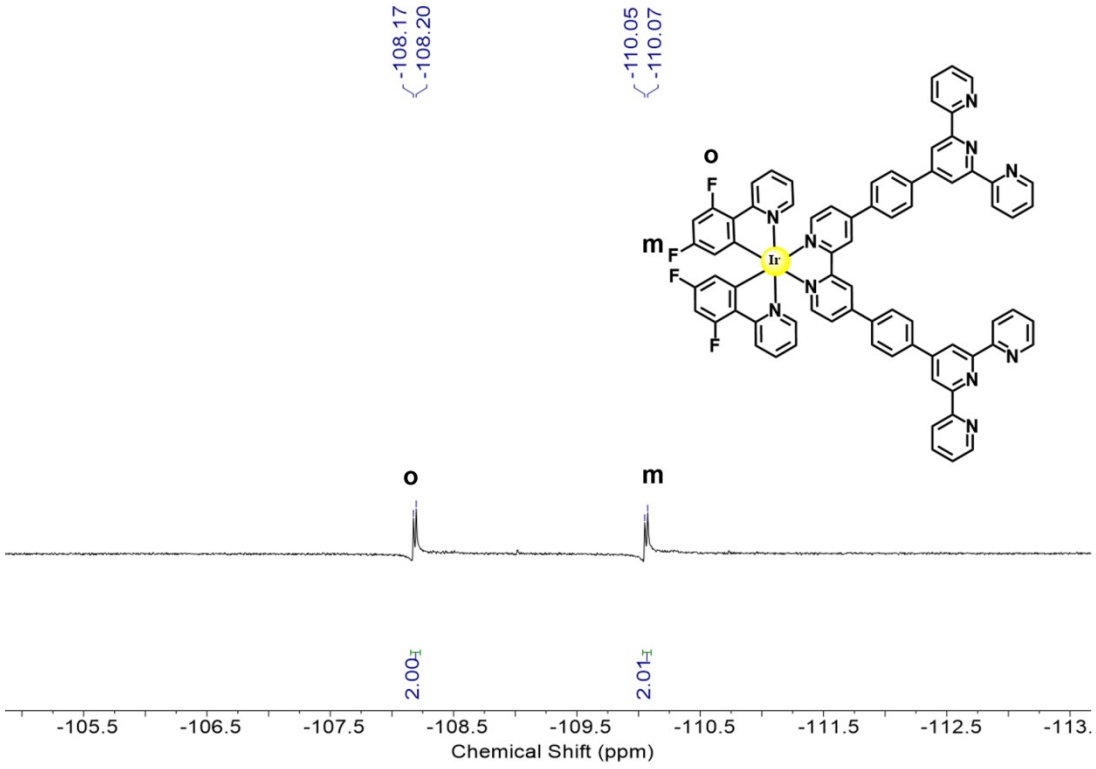

Figure **S12**: ^{19}F NMR spectrum (471 MHz) of ligand **L2** in CD_3CN.

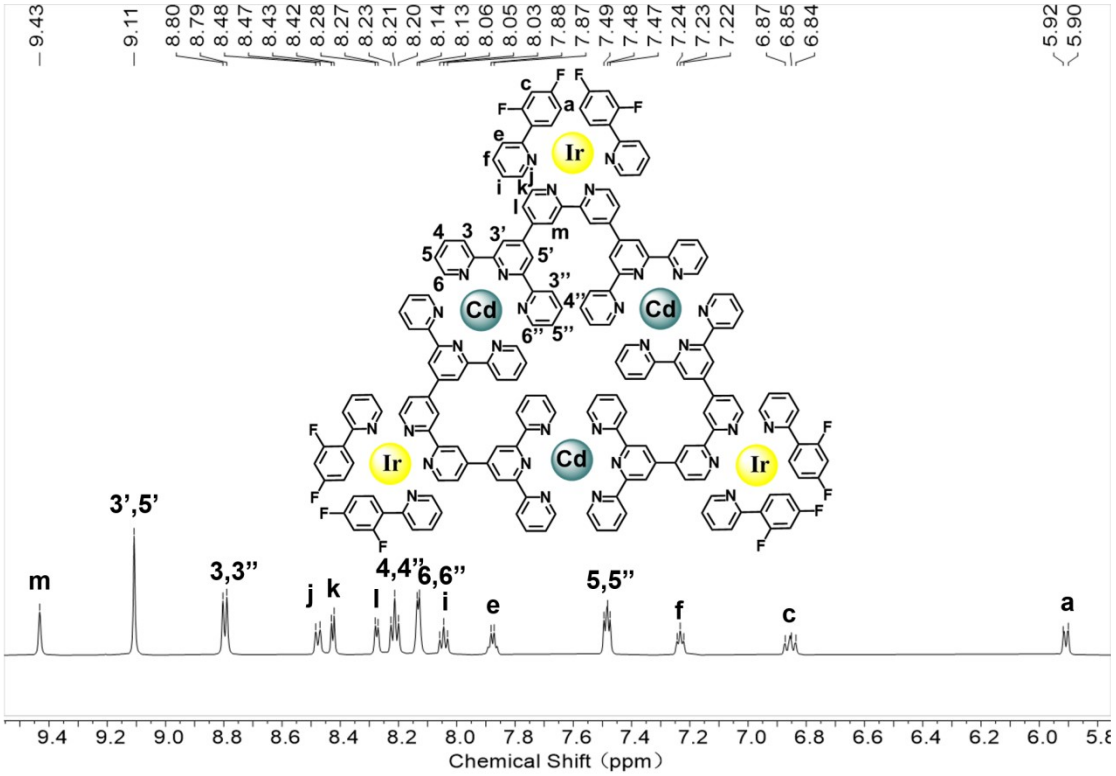

Figure **S13**. ^{1}H NMR spectrum of triangle **S1** (600 MHz, CD_3CN, 298K).

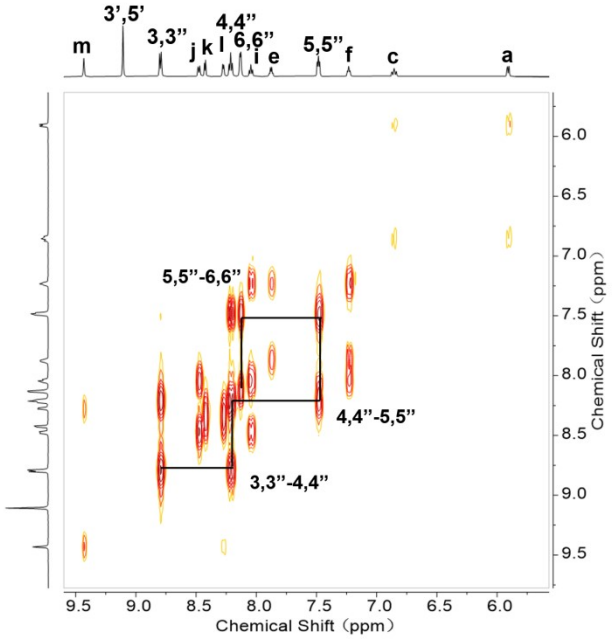

Figure **S14**. 2D COSY spectrum of triangle **S1** (600 MHz, CD_3CN, 298K).

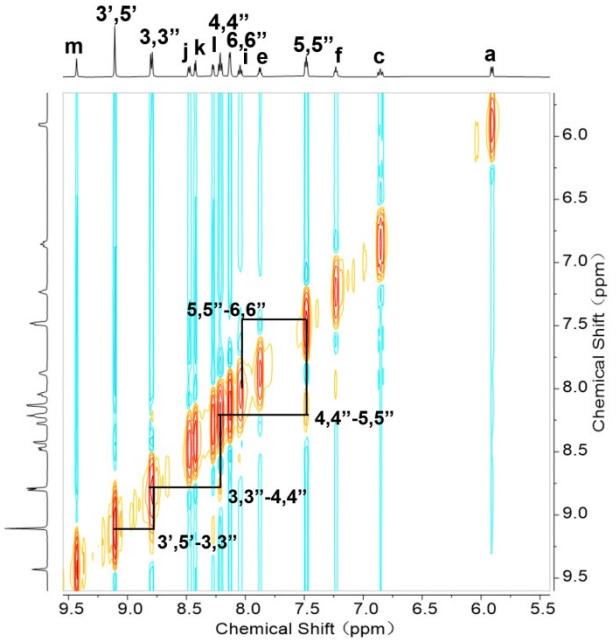

Figure **S15**. 2D NOESY spectrum of triangle **S1** (600 MHz, CD_3CN, 298K).

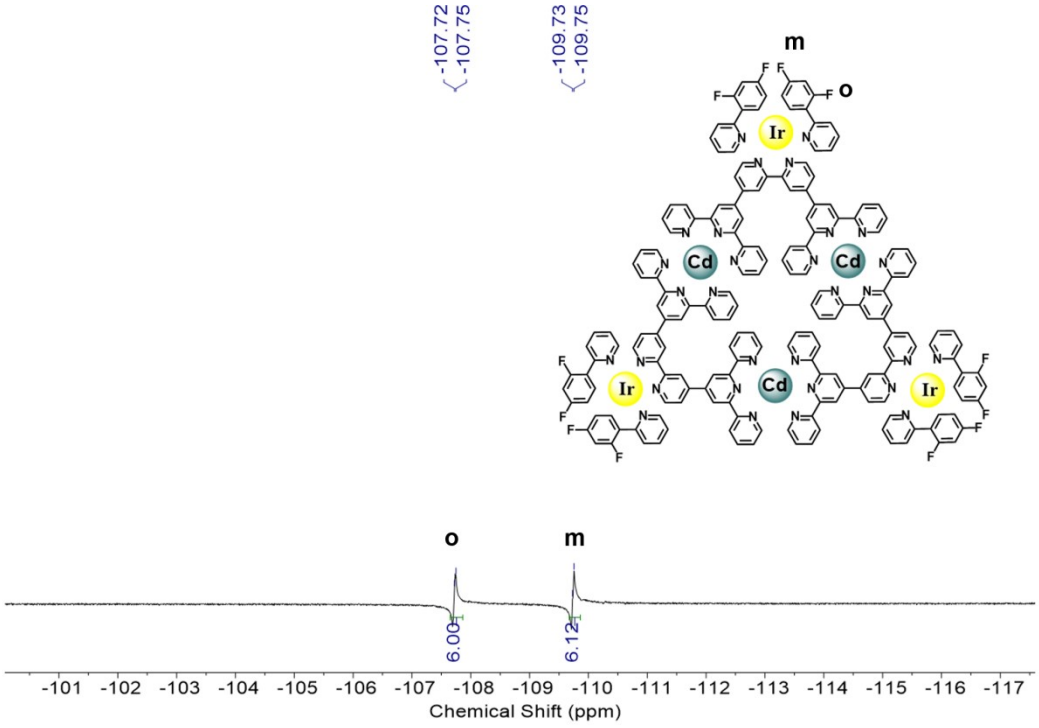

Figure **S16**: ^{19}F NMR spectrum of triangle **S1** (471 MHz, CD_3CN, 298K).

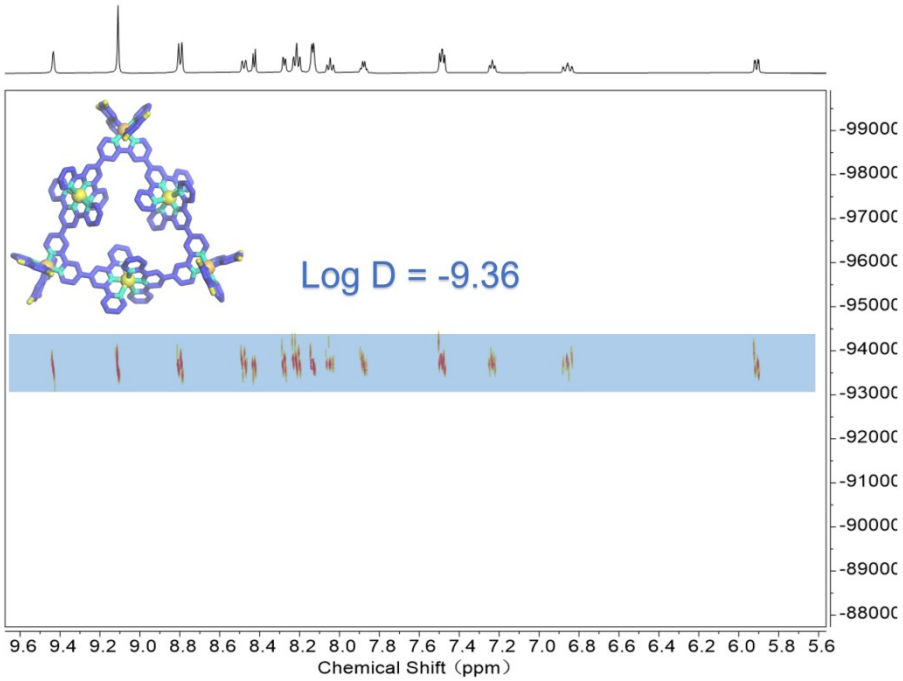

Figure **S17**. DOSY spectrum of triangle **S1** (600 MHz, CD_3CN, 298K).

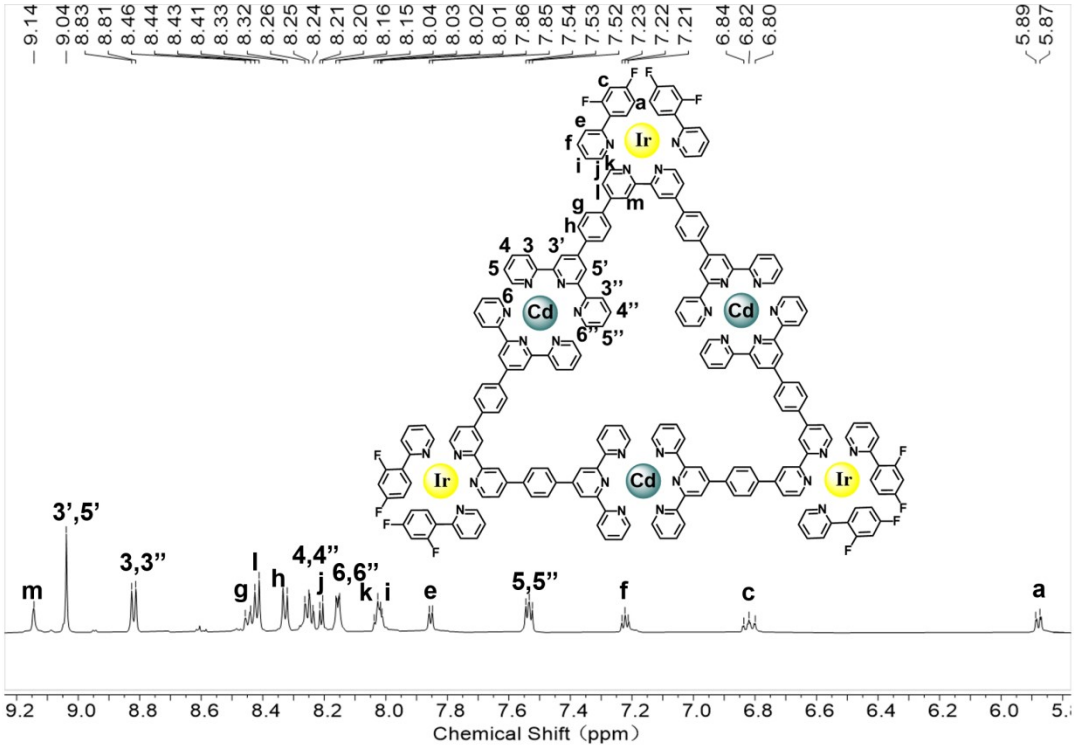

Figure **S18**. ^1H NMR spectrum of triangle **S2** (600 MHz, CD_3CN, 298K).

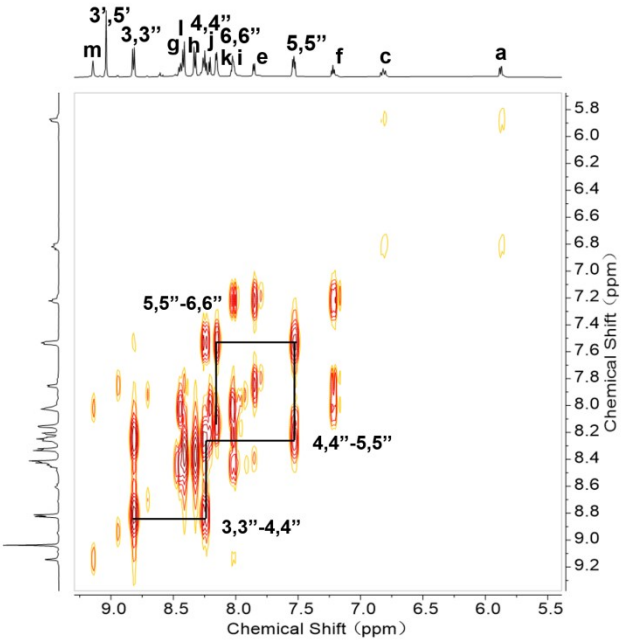

Figure **S19**. 2D COSY spectrum of triangle **S2** (600 MHz, CD_3CN, 298K).

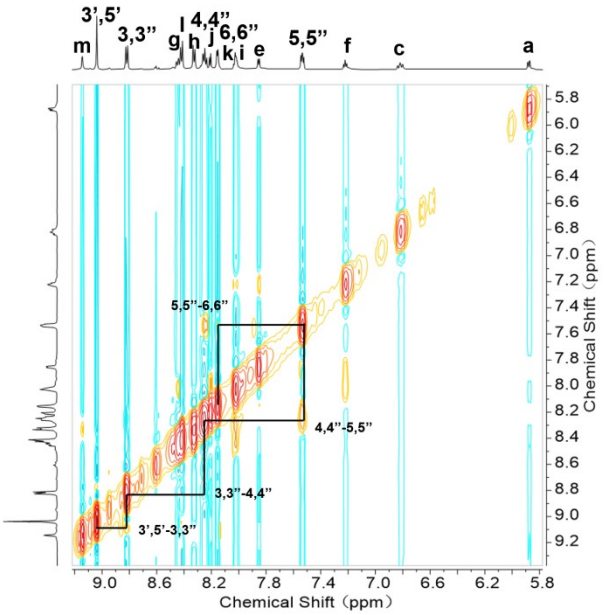

Figure **S20**. 2D NOESY spectrum of triangle **S2** (600 MHz, CD_3CN, 298K).

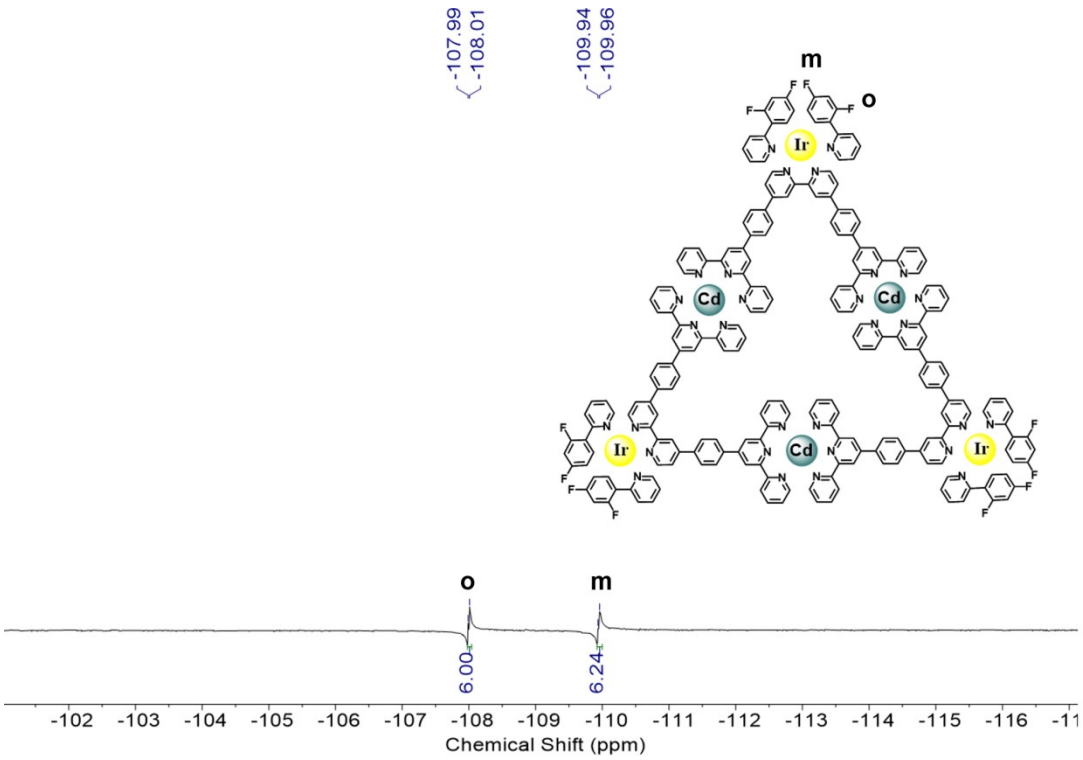

Figure **S21**: ^{19}F NMR spectrum of triangle **S2** (471 MHz, CD_3CN, 298K).

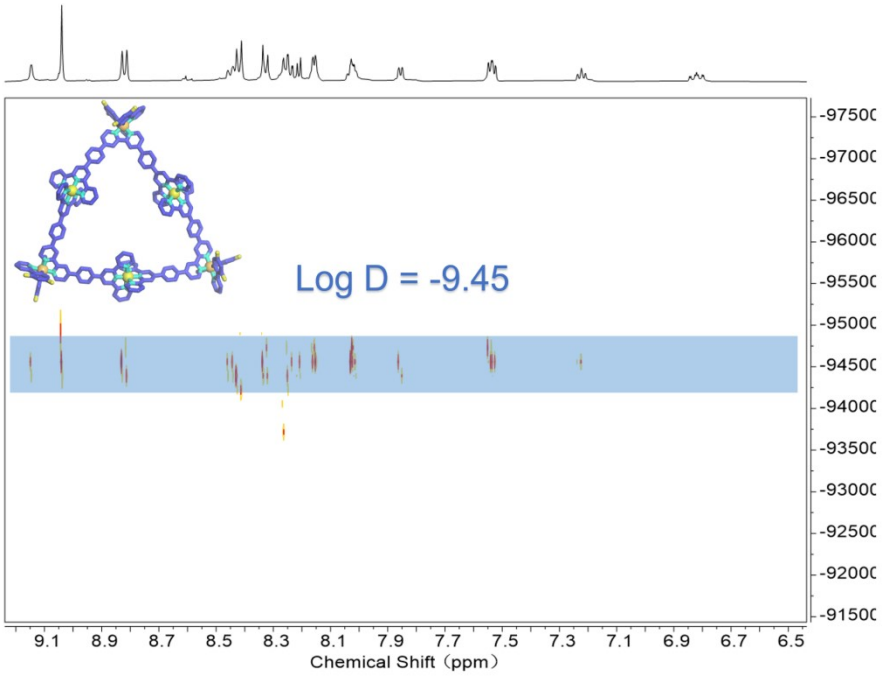

Figure **S22**. DOSY spectrum of triangle **S2** (600 MHz, CD_3CN, 298K).

4. ESI-MS spectra data of ligands and complexes.

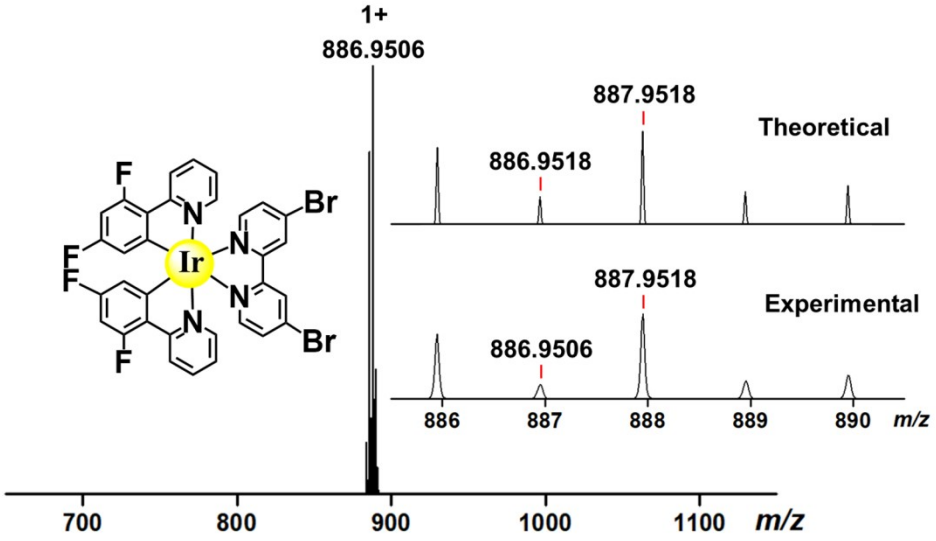

Figure **S23**. ESI-MS spectrum of compound **2** (PF_6^- as counterion).

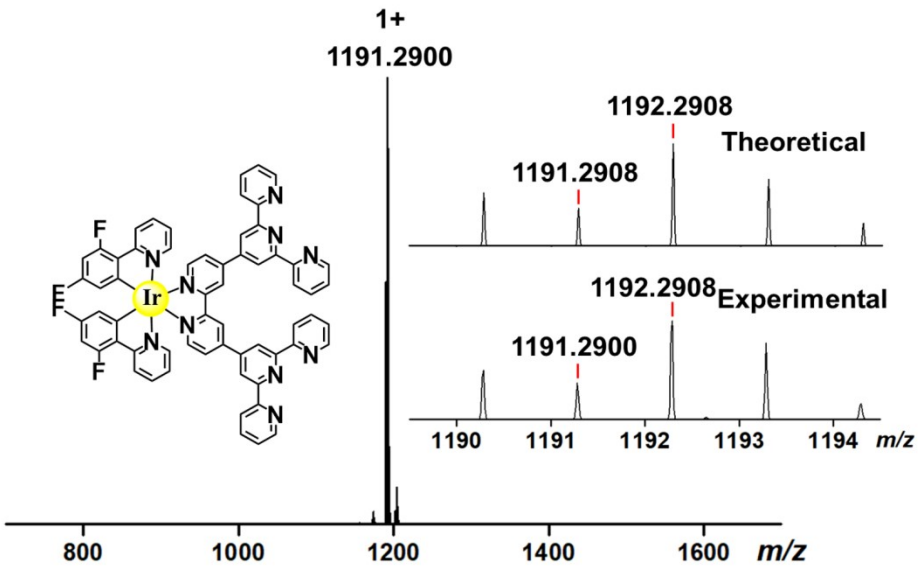

Figure **S24**. ESI-MS spectrum of ligand **L1** (PF_6^- as counterion).

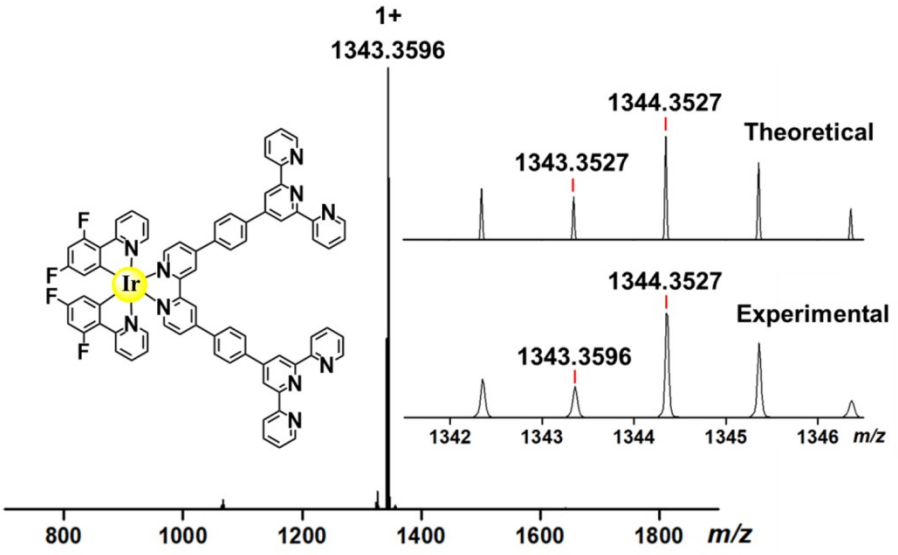

Figure **S25**. ESI-MS spectrum of ligand **L2** (PF_6^- as counterion).

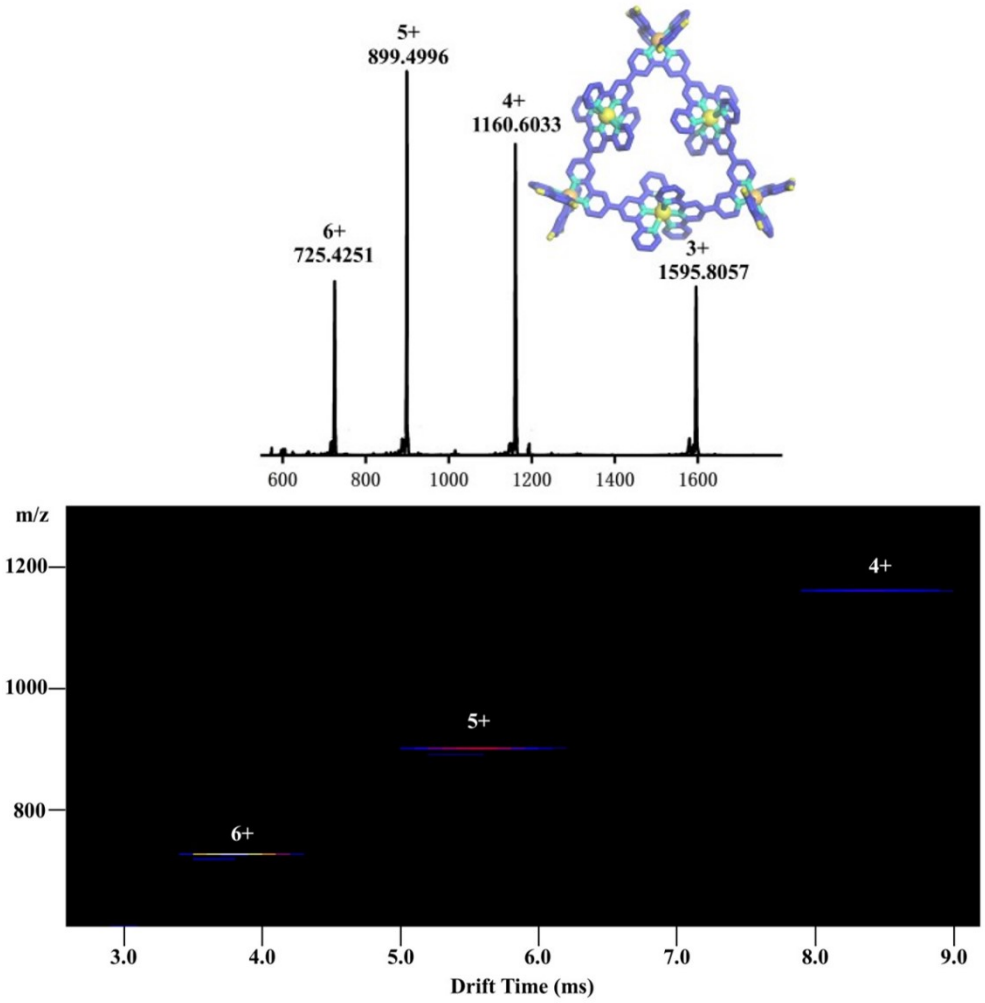

Figure **S26**. ESI-MS spectrum of triangle **S1** (PF_6^- as counterion).

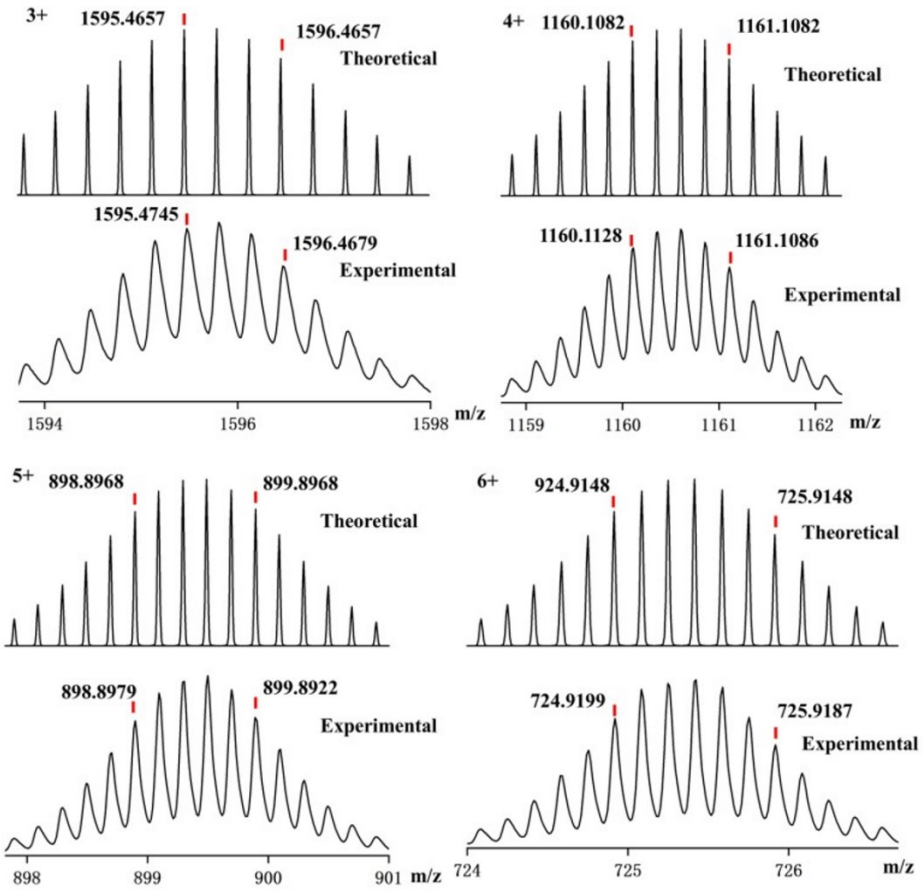

Figure **S27**. Isotope patterns of **S1** (PF_6^- as counterion).

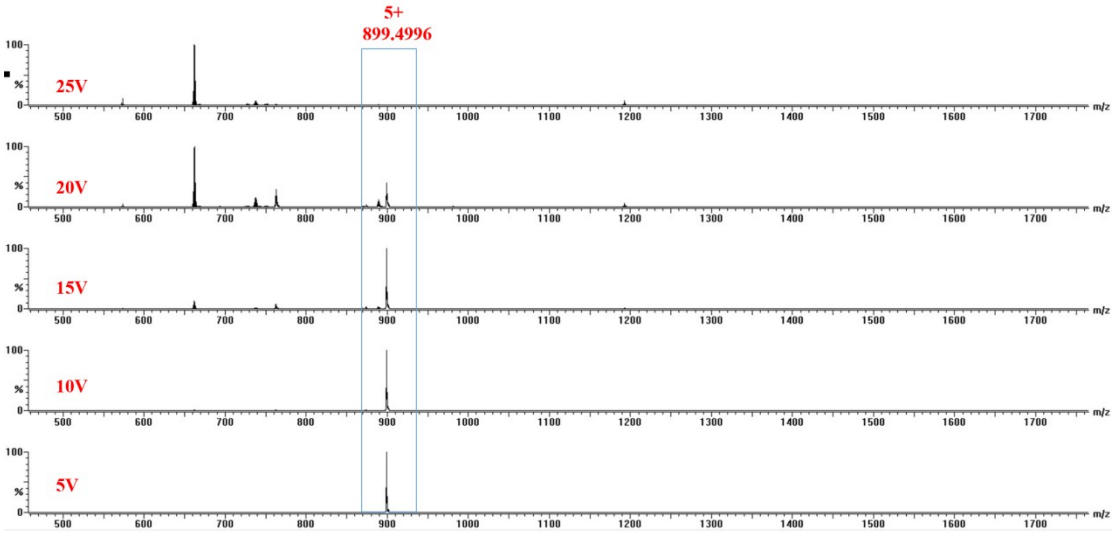

Figure **S28**. gMS**2** of **S1** at m/z 899.4996 (5+) with different collision energies.

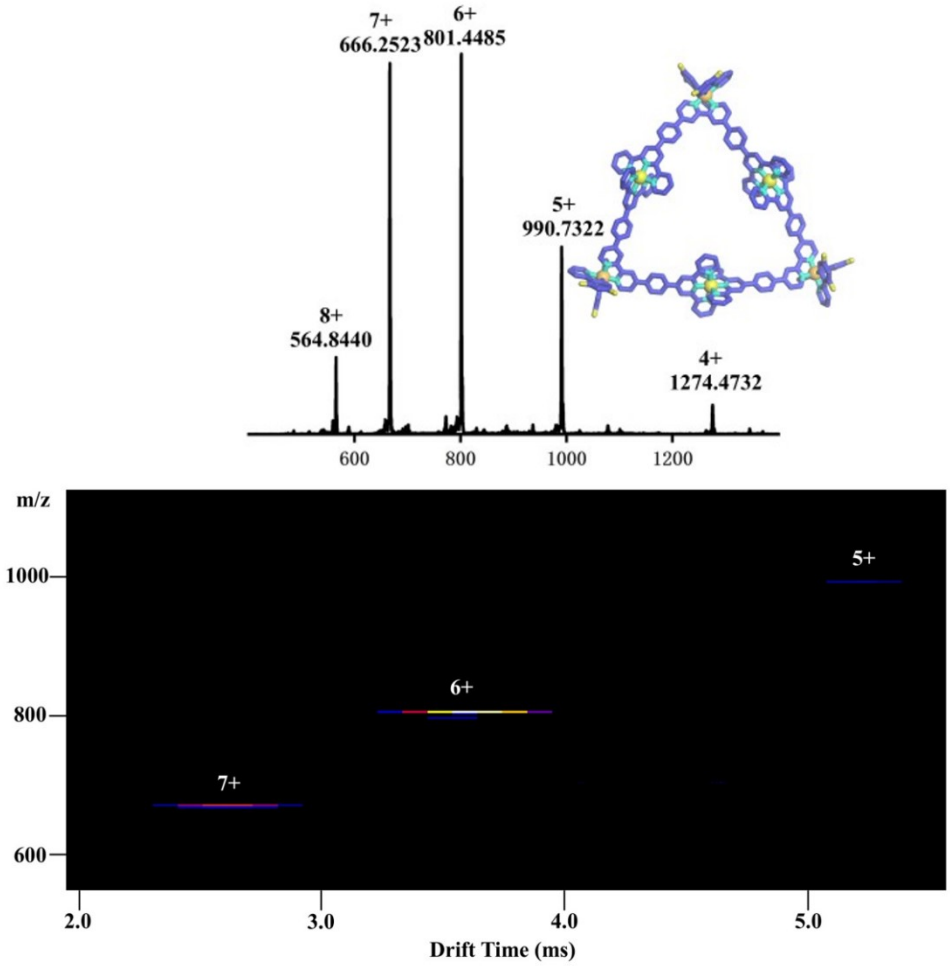

Figure **S29**. ESI-MS spectrum of triangle **S2** (PF_6^- as counterion).

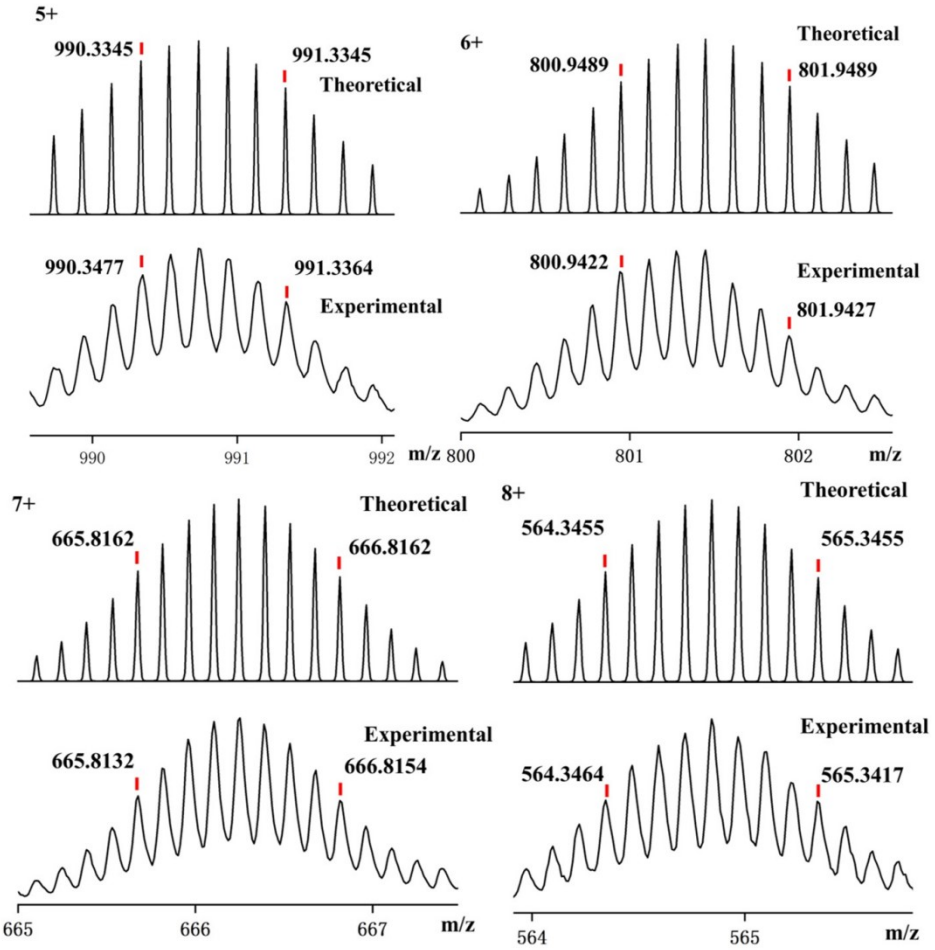

Figure **S30**. Isotope patterns of **S2** (PF_6^- as counterion).

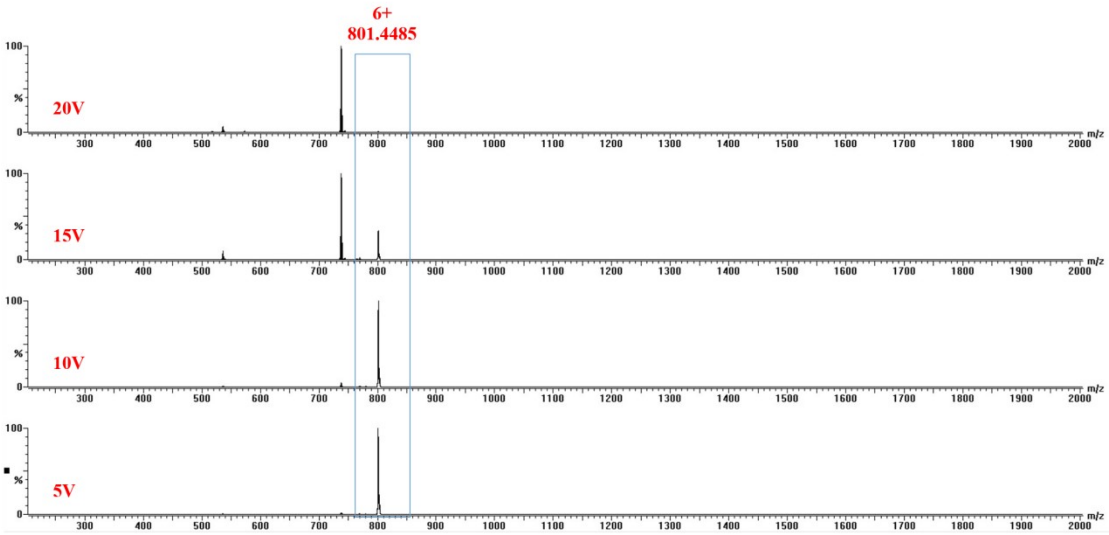

Figure **S31**. gM**S2** of **S2** at m/z 801.4485 (6+) with different collision energies.

5. Photocatalytic degradation of Rhodamine B

To investigate the photocatalytic degradation efficiency of supramolecular architectures **S1** and **S2** toward Rhodamine B (Rh B), stock solutions were prepared as follows: **S1** and **S2** were dissolved in acetonitrile to a concentration of 4×10^{-5} M, and RhB was dissolved in acetonitrile to 4×10^{-4} M. Five 5 mL glass vials were used. Three vials received 2.5 mL of the Rh B solution; among these, to one vial, 0.1 mL of acetonitrile was added as a blank control, while to the other two vials, 0.1 mL of the above-prepared **S1** and **S2** solutions were added, respectively. The remaining two vials contained 0.1 mL of **S1** or **S2** solution diluted with 2.5 mL of acetonitrile, serving as catalyst-only controls.

All samples were placed in a multi-channel photocatalytic reactor and irradiated with white light (250 mW/cm^2) for 0–10 minutes. UV-Vis absorption spectra were recorded at 1-minute intervals. The degradation efficiency (η) was calculated using the equation: $\eta = (A_0 – A)/A_0 \times 100\%$, where A_0 and A represent the initial and time-dependent absorbance of RhB at 554 nm, respectively.

Under light irradiation, Rh B alone exhibited approximately 30% self-degradation (Figure S29). In contrast, in the presence of **S1** and **S2**, the degradation efficiencies reached 82.5% and 84.9% within 10 minutes, respectively, demonstrating the remarkable photocatalytic activity of these iridium-based metallo-organic triangles (Figures S30-31). In the control experiments containing only the supramolecules (without Rh B), negligible changes in UV-Vis absorption were observed after light irradiation, suggesting that both **S1** and **S2** are photostable under the experimental conditions (Figure S32-33).

To compare the degradation efficiencies of ligands and supramolecular systems, ligands L1 and L2 were used to investigate the degradation of Rhodamine B under the same illumination conditions and using the same method described above. In the presence of L1 and L2, the degradation efficiencies within 10 minutes were 70.0% and 70.6%, respectively (Figs. S39 – S40).

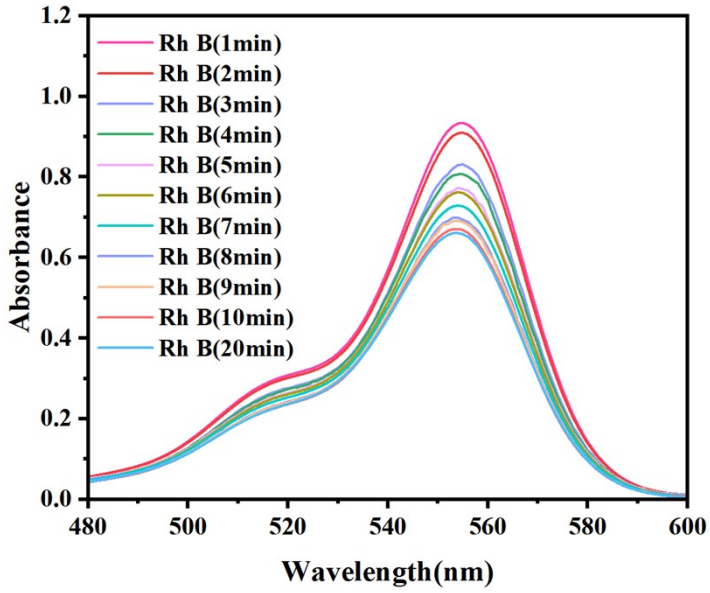

Figure **S32**: Time-dependent absorbance change of Rhodamine B without catalyst irradiating with white light (250 mW/cm^2).

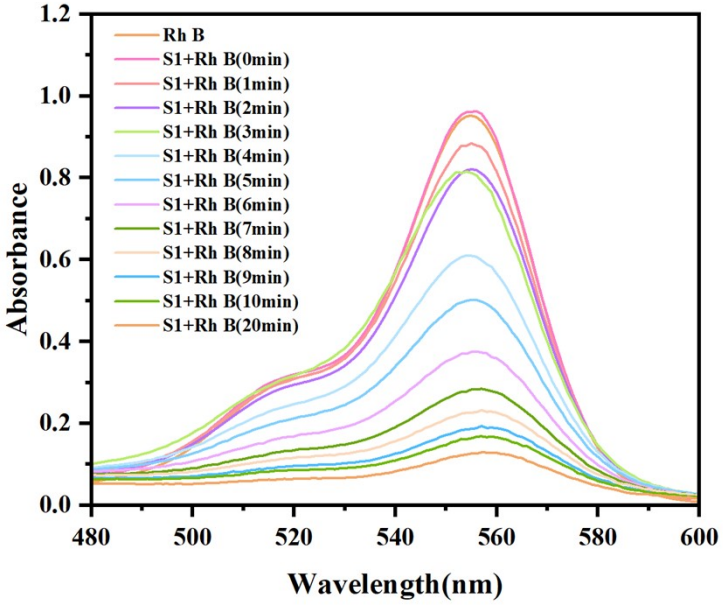

Figure **S33**: Time-dependent changes in the absorbance of Rhodamine B in the presence of **S1** irradiating with white light (250 mW/cm^2).

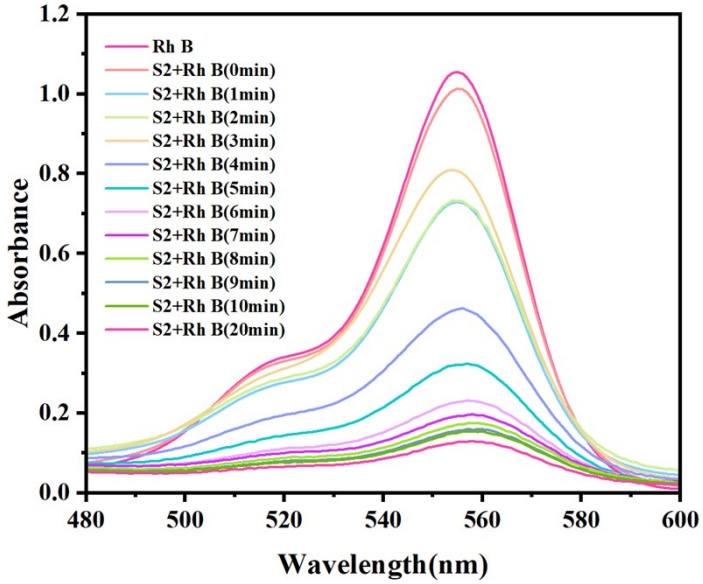

Figure **S34**: Time-dependent changes in the absorbance of Rhodamine B in the presence of **S2** irradiating with white light (250 mW/cm^2).

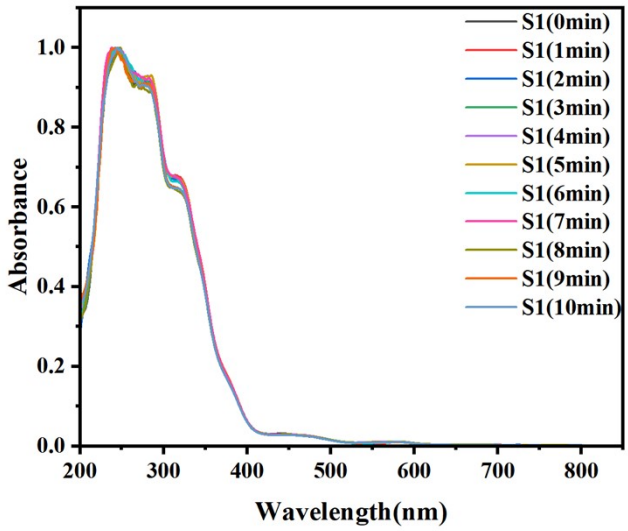

Figure **S35**: Time-dependent absorbance change of supramolecule **S1** irradiating with white light (250 mW/cm^2).

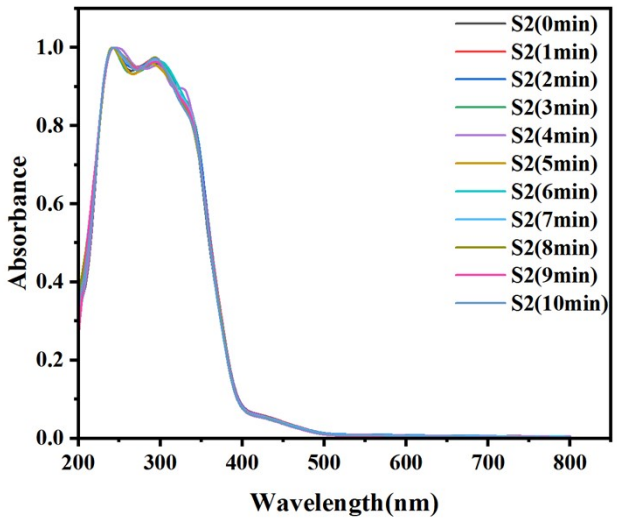

Figure **S36**: Time-dependent absorbance change of supramolecule **S2** irradiating with white light (250 mW/cm^2).

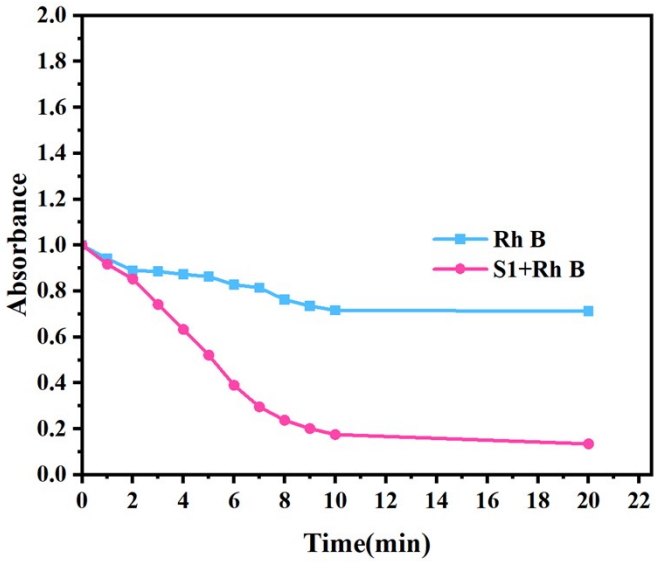

Figure **S37**: Time-dependent changes in the normalized UV-Vis absorbance of Rhodamine B at 554 nm in the absence (blue line) and presence of **S1** (pink line).

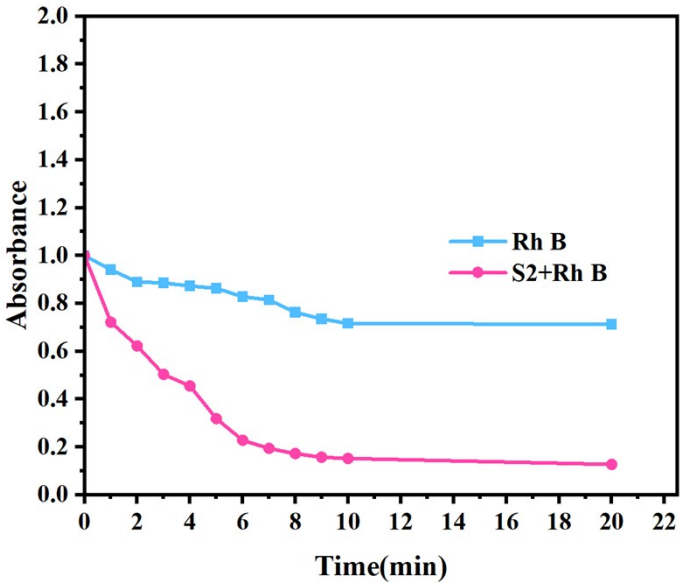

Figure **S38**: Time-dependent changes in the normalized UV-Vis absorbance of Rhodamine B at 554 nm in the absence (blue line) and presence of **S2** (pink line).

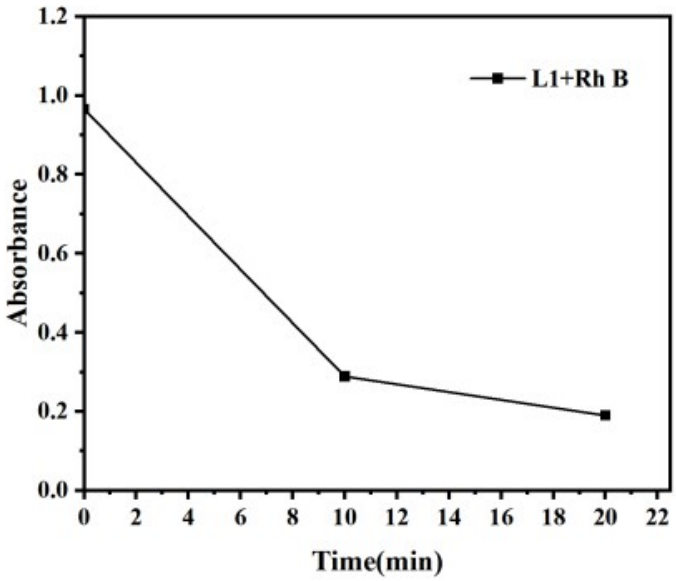

Figure **S39**: The variation of the ultraviolet-visible absorbance of Rhodamine B at 554 nm with time in the presence of **L1**.

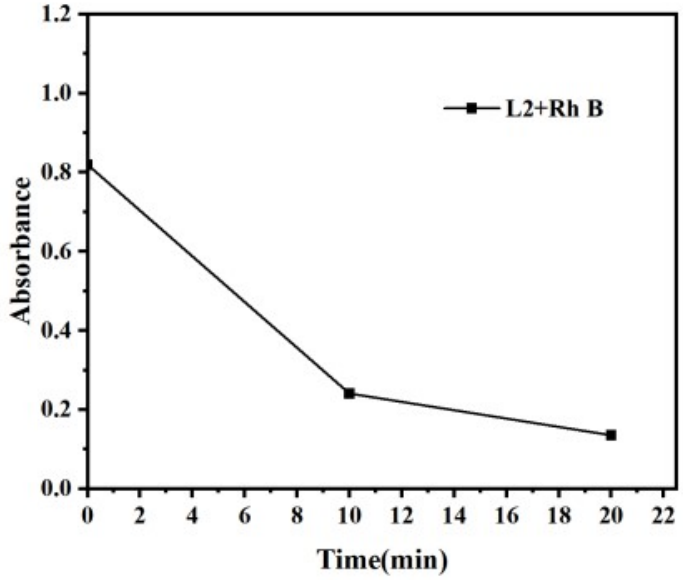

Figure **S40**: The variation of the ultraviolet-visible absorbance of Rhodamine B at 554 nm with time in the presence of **L2**.

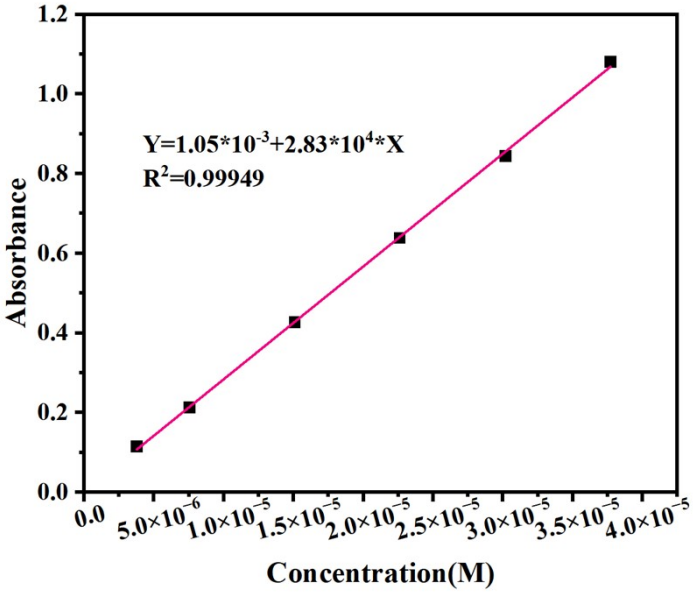

Figure **S41**: Standard curves of Rhodamine B versus the absorbance.

Table **S1** Comparison with reported photodegradation of rh b photocatalysts.

System	Degradation efficiency	Ref.
Copper-doped zinc oxide nanoparticles	100% degradation efficiency within 120 minutes	2
Zinc-based metal-organic framework material [Zn (bdc)(bpb)]$_n$	94.3% degradation efficiency within 45 minutes	3
Z-type heterojunction photocatalyst C-TiO_2/g-C_3N_5(CTCN)	96.6% degradation efficiency within 90 minutes	4
Vanadium-titanium magnetite tailings/quartz sand composite material	98% degradation rate within 20 minutes	5
CdS QDs@ZnO/ZnCr-CO_3-LDH	Degradation efficiency of 98.26% within 180 minutes	6
a nitrogen-doped porous carbon-supported Co-Fe-NC(4:2) catalyst added to PMS	100% degradation efficiency within 6 minutes	7
MMT-supported TiO_2 nanotubes	90% degradation efficiency within 210 minutes	8

6. References

1. S. Sprouse, K. A. King, P. J. Spellane and R. J. Watts, *J. Am. Chem. Soc*, 1984, **106**, 6647–6653.
2. G. Chen, M. Yang, B. Tian, J. Yao, S. Chen, D. Li and G. Yuan, *Sci. Rep*, 2025, **15**, 18246.

3. X. Li, M. Zhang, Y. Yan, H. Sun, M. La, Y. Hu, Q. Jia, Z. Ding, J. Su, C. Chen, Y. Han and S. Ma, *Dalton Trans.*, 2025, **51**, 5151–5163.
4. M. X. Tian, Y. M. Yan, Y. Zhang, T. Y. Cui, G. Y. Zhang, J. B. Zhao, Y. Y. Yang and J. H. Jiang, *Inorg. Chem. Commun.*, 2023, **158**.
5. Y. Liu, C. Liao, L. Liu, X. Zhu, Z. Chen, D. Ren, T. Yang and Y. Sun, *Miner. Eng.*, 2024, **219**, 109083.
6. N. M. Abdelbar, M. A. Ahmed and A. A. Mohamed, *Opt. Mater.*, 2024, **155**, 115802.
7. D. P. Jaihindh, S.-B. Lu, T.-T. Chang, Y.-F. Lin, K. Shukla, T.-F. M. Chang, M. Sone and C.-Y. Chen, *ACS Appl. Nano Mater.*, 2025, **8**, 17154–17164.
8. T. B. T. Dao, T. T. L. Ha, T. D. Nguyen, H. N. Le, C. N. Ha-Thuc, T. M. L. Nguyen, P. Perre and D. M. Nguyen, *Chemosphere*, 2021, **280**, 130802.